

# Efficient asymmetric collisional Brownian particle engines

C. E. Fernández Noa,<sup>1</sup> Angel L. L. Stable,<sup>1</sup> William G. C. Oropesa,<sup>1</sup> Alexandre Rosas,<sup>2</sup> and C. E. Fiore<sup>1</sup>

<sup>1</sup>*Instituto de Física da Universidade de São Paulo, 05508-090 São Paulo, SP, Brazil*

<sup>2</sup>*Departamento de Física, CCEN, Universidade Federal da Paraíba, Caixa Postal 5008, 58059-900, João Pessoa, Brazil*

(Dated: August 4, 2021)

The construction of efficient thermal engines operating at finite times constitutes a fundamental and timely topic in nonequilibrium thermodynamics. We introduce a strategy for optimizing the performance of Brownian engines, based on a collisional approach for unequal interaction times between the system and thermal reservoirs. General (and exact) expressions for thermodynamic properties and their optimized values are obtained, irrespective of the driving forces, asymmetry, the temperatures of reservoirs and protocol to be maximized. Distinct routes for the engine optimization, including maximizations of output power and efficiency with respect to the asymmetry, force and both of them are investigated. For the isothermal work-to-work converter and/or small difference of temperature between reservoirs, they are solely expressed in terms of Onsager coefficients. Although the symmetric engine can operate very inefficiently depending on the control parameters, the usage of distinct contact times between the system and each reservoir not only can enhance the machine performance (signed by an optimal tuning ensuring the largest gain) but also enlarges substantially the machine regime operation. The present approach can pave the way for the construction of efficient Brownian engines operating at finite times.

## I. INTRODUCTION

A long-standing dilemma in Thermodynamics and related areas concerns the issue of mitigating the impact of thermal noise/wasted heat in order to improve the machine performance. This constitutes a high relevant problem, not only for theoretical purposes but also for the construction of experimental setups [1–3]. Giving that the machine performance is commonly dependent on particular chemical compositions and operation conditions, notably for small-scale engines, the role of fluctuations being crucial for such engines, distinct approaches have been proposed and investigated in the realm of stochastic and quantum thermodynamics [4, 5]. A second fundamental point concerns that, even if all sources of dissipation could be mitigated, the performance of any thermal machine would still be limited by Carnot efficiency, which requires the occurrence of infinitely slow quasi-static processes and consequently the engine operates at null power. In contrast, realistic systems operate at finite time and power. Such conundrum (control/mitigation of dissipation and engine optimization) has contributed for the discovery of several approaches based on the maximization of power output instead of the efficiency [4–20].

Thermal machines based on Brownian particles have been successfully studied not only for theoretical purposes [6, 7, 15, 21] but also for the building of reliable experimental setups [22–27]. They are also remarkable for depicting the limitations of classical thermodynamics and disclose the scales in which thermal fluctuations become relevant. In several situations, thermal machines involve isothermal transformations [22, 23, 25]. Such class of processes are fundamental in thermodynamic since they are minimally dissipative. However, isothermal transformations are slow, demanding sufficient large number of stages for achieving the desired final state. For this reason, distinct protocols, such as increasing the coupling between system and the thermal bath, have been undertaken for speeding it up and simultaneously controlling the increase of dissipation [28–32].

Here we introduce a strategy for optimizing the performance of irreversible Brownian machines operating at isothermal parts via the control of interaction time between the system and the environment. Our approach is based on a Brownian particle sequentially placed in contact with distinct thermal baths and subject to external forces [33] for unequal times. Such description, also referred as collisional, has been successfully employed in different contexts, such as systems that interact only with a small fraction of the environment and those presenting distinct drivings over each member of system [34–37]. Depending on the parameters of the model (period, driving and difference of temperatures), the symmetric version can operate very inefficiently. Our aim is to show that the machine performance improves substantially by tuning properly the interaction time between particle and each reservoir. Besides the increase of the power and/or efficiency, the asymmetry in the contact time also enlarges the regime of operation of the machine substantially. Contrasting with previous works [29–32], the optimization is solely obtained via the control of interaction time and no external parameters are considered. We derive general relations for distinct kinds of maximization, including the maximization of the efficiency and power with respect to the force, the asymmetry and both of them. For the isothermal work-to-work converter and/or small difference of temperature between reservoirs, they are solely expressed in terms of Onsager coefficients. The present approach can pave the way for the construction of efficient Brownian engines operating at finite times.

This paper is organized as follows: In Sec. II we present the thermodynamic of Brownian particles subject to asymmetric time switching. In Sec. III, the efficiency is analyzed for two cases: the work-to-work converter processes and distinct temperature reservoirs. Optimization protocols are presented and exemplified for distinct drivings. Finally, conclusions are drawn in Sec. IV and explicit calculations of Onsager coefficients and linear regimes are present in Appendixes.

## II. THERMODYNAMICS OF ASYMMETRIC INTERACTION TIMES

We consider a Brownian particle with mass  $m$  sequentially and cyclically placed in contact with different thermal reservoirs, each at a temperature  $T_i$  for time interval  $\tau_i$ . Here  $i = 1, \dots, N$  label the reservoirs and also the order of contact between the reservoirs and the particle. While in contact with the  $i$ -th reservoir, the velocity  $v_i(t)$  of the particle evolves in time according to the Langevin equation

$$\frac{dv_i}{dt} = -\gamma_i v_i + f_i(t) + \zeta_i(t), \quad (1)$$

where  $\gamma_i$ ,  $f_i(t)$  and  $\zeta_i(t)$  denote, respectively, the viscous constants, external forces and stochastic forces (interaction between particle and the  $i$ -th reservoir), all divided by the mass of the particle. Stochastic forces are assumed to satisfy the white noise properties:

$$\langle \zeta_i(t) \rangle = 0, \quad (2)$$

and,

$$\langle \zeta_i(t) \zeta_{i'}(t') \rangle = 2\gamma_i T_i \delta_{ii'} \delta(t - t'). \quad (3)$$

The system evolves to a nonequilibrium steady state regime (*NESS*) characterized by a non-vanishing production of entropy. The time evolution of the velocity probability distribution at time  $t$ ,  $P_i(v, t)$ , is described by the Fokker-Planck equation [38–40]

$$\frac{\partial P_i}{\partial t} = -\frac{\partial J_i}{\partial v} - f_i(t) \frac{\partial P_i}{\partial v}, \quad (4)$$

where  $J_i$  is the probability current

$$J_i = -\gamma_i v P_i - \frac{\gamma_i k_B T_i}{m} \frac{\partial P_i}{\partial v}. \quad (5)$$

As can be verified by direct substitution, the *NESS* is characterized by a Gaussian probability distribution  $P_i(v, t)$ :

$$P_i(v, t) = \frac{1}{\sqrt{2\pi b_i(t)}} e^{-\frac{(v - \langle v_i \rangle)^2}{2b_i(t)}}, \quad (6)$$

for which the mean  $\langle v_i \rangle(t)$  and the variance  $b_i(t) \equiv \langle v_i^2 \rangle(t) - \langle v_i \rangle^2(t)$  are time-dependent and obey the following equations of motion

$$\frac{d}{dt} \langle v_i \rangle(t) = -\gamma_i \langle v_i \rangle(t) + f_i(t), \quad (7)$$

and

$$\frac{d}{dt} b_i(t) = -2\gamma_i b_i(t) + \Gamma_i, \quad (8)$$

where  $\Gamma_i = 2\gamma_i k_B T_i / m$ . Obviously, the continuity of the probability distribution must be assured, and we will use it to calculate  $b_i(t)$  and  $\langle v_i \rangle(t)$  in the following sections.

In order to derive explicit expressions for macroscopic quantities, we start from the definitions of the average energy

$U_i = m \langle v_i^2 \rangle / 2$  and entropy  $S_i(t) = -k_B \langle \ln[P_i(v, t)] \rangle$ , respectively. In both cases, the time variation can be straightforwardly obtained from the Fokker-Planck equation and applying vanishing boundary conditions for both  $P_i(v, t)$  and  $J_i(v, t)$  in the infinity speed limit [38]. The former is related with the average power dissipated  $\dot{W}_i$  and the heat dissipation during the same period  $\dot{Q}_i$  through the first law of thermodynamics relation:

$$\frac{dU_i}{dt} = -[\dot{W}_i(t) + \dot{Q}_i(t)], \quad (9)$$

where  $\dot{W}_i(t)$  and  $\dot{Q}_i(t)$  are given by the following expressions:

$$\dot{W}_i(t) = -m \langle v_i \rangle(t) f_i(t), \quad (10)$$

and

$$\dot{Q}_i(t) = m\gamma_i \left( \langle v_i^2 \rangle(t) - \frac{\Gamma_i}{2\gamma_i} \right). \quad (11)$$

Similarly, the rate of variation of the entropy can be written as [39, 40]:

$$\frac{dS_i}{dt} = \Pi_i(t) - \Phi_i(t), \quad (12)$$

where  $\Pi_i(t)$  and  $\Phi_i(t)$  denote the entropy production rate and the flux of entropy, respectively, which expressions are given by,

$$\Pi_i(t) = \frac{2k_B}{\Gamma_i} \int \frac{J_i^2}{P_i} dv, \quad (13)$$

and

$$\Phi_i(t) = -\frac{2\gamma_i k_B}{\Gamma_i} \int v J_i dv = \frac{2\gamma_i k_B \dot{Q}_i(t)}{m\Gamma_i} = \frac{\dot{Q}_i(t)}{T_i}. \quad (14)$$

Both expressions are valid during the contact of the Brownian particle with the  $i$ -th reservoir.

As stated before, the present collisional approach for Brownian machines can be considered for an arbitrary set of reservoirs and external forces, which generic solutions  $\langle v_i \rangle(t)$ 's and  $b_i(t)$ 's in the nonequilibrium steady state regime are

$$\langle v_i \rangle(t) = e^{-\gamma_i(t - \tilde{\tau}_{i-1})} a_i + e^{-\gamma_i t} F_i(t), \quad (15)$$

and

$$b_i(t) = A_i e^{-2\gamma_i(t - \tilde{\tau}_{i-1})} + \frac{\Gamma_i}{2\gamma_i}, \quad (16)$$

respectively, where  $\tilde{\tau}_i = \sum_{j=1}^i \tau_j$  (with  $\tau_0 \equiv 0$ ),  $a_i$  and  $A_i$  are integration constants to be determined from the boundary conditions and  $F_i(t)$  can be viewed as a ‘‘time integrated force’’, which is related to the external forces through the expression

$$F_i(t) = \int_{\tilde{\tau}_{i-1}}^t e^{\gamma_i t'} f_i(t') dt'. \quad (17)$$

Here, the variable  $t$  is interpreted as the time modulus the period  $\tau = \tilde{\tau}_N$ .

Since the probability distribution is continuous, the conditions  $\langle v_i \rangle(\tau_i) = \langle v_{i+1} \rangle(\tau_i)$  and  $b_i(\tau_i) = b_{i+1}(\tau_i)$  must hold for  $i = 1, \dots, N-1$ . In addition, the steady state condition (periodicity) implies that  $\langle v_1 \rangle(0) = \langle v_N \rangle(\tau)$  and  $b_1(0) = b_N(\tau)$ . Hence, the  $a_i$  and  $A_i$  can be determined as the solution of two uncoupled linear systems of  $N$  equations each. Here we shall focus on the case of  $N = 2$  reservoirs – the simplest case for tackling the efficiency of a thermal engine, in which the interaction with the first and second reservoirs occur during  $\tau_1$  and  $\tau_2 = \tau - \tau_1$ , respectively. For simplicity, from now on, we consider that the viscous constant are equal  $\gamma_1 = \gamma_2 = \gamma$ . Therefore, the average velocities and their variances are

$$\begin{aligned} \langle v_1 \rangle(t) &= \frac{(e^{\gamma\tau} - 1)F_1(t) + F_1(\tau_1) + F_2(\tau)}{e^{\gamma t}(e^{\gamma\tau} - 1)}, \\ \langle v_2 \rangle(t) &= \frac{e^{\gamma\tau}F_1(\tau_1) + (e^{\gamma\tau} - 1)F_2(t) + F_2(\tau)}{e^{\gamma t}(e^{\gamma\tau} - 1)}, \end{aligned} \quad (18)$$

and

$$\begin{aligned} b_1(t) &= -\frac{(\Gamma_1 - \Gamma_2)(1 - e^{-2\gamma\tau_2})}{2\gamma(1 - e^{-2\gamma\tau})}e^{-2\gamma t} + \frac{\Gamma_1}{2\gamma}, \\ b_2(t) &= \frac{(\Gamma_1 - \Gamma_2)(1 - e^{-2\gamma\tau_1})}{2\gamma(1 - e^{-2\gamma\tau})}e^{-2\gamma(t-\tau_1)} + \frac{\Gamma_2}{2\gamma}, \end{aligned} \quad (19)$$

respectively. The expressions for  $\langle v_1 \rangle(t)$  and  $b_1(t)$  hold for  $0 \leq t \leq \tau_1$ , while the expressions for  $\langle v_2 \rangle(t)$  and  $b_2(t)$  are valid for  $\tau_1 \leq t \leq \tau$ . It is worth pointing out that the particle will be exposed to the contact with the reservoir 1 and force  $f_1(t)$  for a longer (shorter) time than with reservoir 2 and force  $f_2(t)$  if  $\tau_1 \geq \tau_2$  ( $\tau_1 \leq \tau_2$ ). Furthermore, while the average velocities  $\langle v_i \rangle(t)$  depend on the external force (but not on the temperature of the reservoirs), its variances  $b_i(t)$  depend on the temperatures (but not on the external forces).

Having the expressions for the mean velocities and variances, thermodynamic quantities of interest can be directly obtained. The average work in each part of the cycle is given by

$$\bar{W}_1 = \frac{1}{\tau} \int_0^{\tau_1} \langle v_1 \rangle(t) f_1(t) dt, \quad (20)$$

$$\bar{W}_2 = \frac{1}{\tau} \int_{\tau_1}^{\tau} \langle v_2 \rangle(t) f_2(t) dt. \quad (21)$$

Using Eq. (18) and expressing each external force as  $f_i(t) = X_i g_i(t)$ , with  $X_i$  and  $g_i(t)$  denoting force strength and its driving, respectively, we finally arrive at the following expressions:

$$\begin{aligned} \bar{W}_1 &= -\frac{m}{\tau(e^{\gamma\tau} - 1)} \left[ X_1^2 \left( (e^{\gamma\tau} - 1) \int_0^{\tau_1} g_1(t) e^{-\gamma t} dt \int_0^{\tau_1} g_1(t') e^{\gamma t'} dt' + \int_0^{\tau_1} g_1(t) e^{-\gamma t} dt \int_0^{\tau_1} g_1(t') e^{\gamma t'} dt' \right) \right. \\ &\quad \left. + X_1 X_2 \int_0^{\tau_1} g_1(t) e^{-\gamma t} dt \int_{\tau_1}^{\tau} g_2(t') e^{\gamma t'} dt' \right], \end{aligned} \quad (22)$$

$$\begin{aligned} \bar{W}_2 &= -\frac{m}{\tau(e^{\gamma\tau} - 1)} \left[ X_2^2 \left( \int_{\tau_1}^{\tau} g_2(t) e^{-\gamma t} dt \int_{\tau_1}^{\tau} g_2(t') e^{\gamma t'} dt' + (e^{\gamma\tau} - 1) \int_{\tau_1}^{\tau} g_2(t) e^{-\gamma t} dt \int_{\tau_1}^{\tau} g_2(t') e^{\gamma t'} dt' \right) \right. \\ &\quad \left. + X_1 X_2 e^{\gamma\tau} \int_{\tau_1}^{\tau} g_2(t) e^{-\gamma t} dt \int_0^{\tau_1} g_1(t') e^{\gamma t'} dt' \right]. \end{aligned} \quad (23)$$

The expressions above, Eqs. (22) and (23), are exact and are valid for any kind of drivings  $g_1(t)$  and  $g_2(t)$  and stage duration  $\tau_1$  and  $\tau_2$ . Usually, in the linear regime,  $\bar{W}_i$  is written as the product of a flux  $\mathcal{J}_i = L_{ii}X_i + L_{ij}X_j$  by a force  $X_i$ , that is,  $\bar{W}_i =$

$-k_B T_i \mathcal{J}_i X_i$ . Since in the present case  $\bar{W}_i$  is always bilinear in the forces  $X_i$ , such expression is also valid even far from the linear regime. Thus, the Onsager coefficients  $L_{ij}$  may be written as,

$$\begin{aligned} L_{11} &= \frac{2\gamma}{\Gamma_1 \tau (e^{\gamma\tau} - 1)} \left[ (e^{\gamma\tau} - 1) \int_0^{\tau_1} g_1(t) e^{-\gamma t} dt \int_0^{\tau_1} g_1(t') e^{\gamma t'} dt' + \int_0^{\tau_1} g_1(t) e^{-\gamma t} dt \int_0^{\tau_1} g_1(t') e^{\gamma t'} dt' \right], \\ L_{22} &= \frac{2\gamma}{\Gamma_2 \tau (e^{\gamma\tau} - 1)} \left[ \int_{\tau_1}^{\tau} g_2(t) e^{-\gamma t} dt \int_{\tau_1}^{\tau} g_2(t') e^{\gamma t'} dt' + (e^{\gamma\tau} - 1) \int_{\tau_1}^{\tau} g_2(t) e^{-\gamma t} dt \int_{\tau_1}^{\tau} g_2(t') e^{\gamma t'} dt' \right], \\ L_{12} &= \frac{2\gamma}{\Gamma_1 \tau (e^{\gamma\tau} - 1)} \int_0^{\tau_1} g_1(t) e^{-\gamma t} dt \int_{\tau_1}^{\tau} g_2(t') e^{\gamma t'} dt', \\ L_{21} &= \frac{2\gamma e^{\gamma\tau}}{\Gamma_2 \tau (e^{\gamma\tau} - 1)} \int_0^{\tau_1} g_1(t') e^{\gamma t'} dt' \int_{\tau_1}^{\tau} g_2(t) e^{-\gamma t} dt. \end{aligned} \quad (24)$$

Reciprocal relations are verified as follows: Since forces  $f_1(t)$

and  $f_2(t)$  solely act from 0 to  $\tau_1$  and  $\tau_1$  to  $\tau$ , respectively, both

upper and lower integral limits in Eqs. (20) and Eq. (21) can be replaced for  $\tau$  and 0, respectively and hence all expressions from Eq. (20) to Eq. (24) can be evaluated over a complete cycle. By exchanging the indexes  $1 \leftrightarrow 2$ , we verify that  $L_{ij} \leftrightarrow L_{ji}$ .

Similarly, general expressions can be obtained for the average heat dissipation during the contact of the Brownian particle with each reservoir. Since the heat is closely related to the entropy production rate [see e.g. Eq. (14)], we curb our discussion to the latter quantity. The average entropy production over a complete cycle is then given by,

$$\bar{\Pi} = \frac{1}{\tau} \left[ \int_0^{\tau_1} \Phi_1(t) dt + \int_{\tau_1}^{\tau} \Phi_2(t) dt \right]. \quad (25)$$

By inserting Eq. (14) into Eq. (25) and using Eq. (11),  $\bar{\Pi}$  can be decomposed in two terms: one associated with the difference of temperature of the reservoirs

$$\bar{\Pi}_T = \frac{k_B}{\tau} \left[ \frac{2\gamma^2}{\Gamma_1} \int_0^{\tau_1} b_1(t) dt + \frac{2\gamma^2}{\Gamma_2} \int_{\tau_1}^{\tau} b_2(t) dt - \gamma\tau \right], \quad (26)$$

and the other coming from the external forces

$$\bar{\Pi}_F = \frac{k_B}{\tau} \left[ \frac{2\gamma^2}{\Gamma_1} \int_0^{\tau_1} \langle v_1 \rangle^2(t) dt + \frac{2\gamma^2}{\Gamma_2} \int_{\tau_1}^{\tau} \langle v_2 \rangle^2(t) dt \right]. \quad (27)$$

Now, from Eqs. (19) and (26), one obtains the general form for  $\bar{\Pi}_T$ :

$$\bar{\Pi}_T = k_B \frac{\Gamma_1 \Gamma_2}{\tau} \frac{\sinh(\gamma\tau_1) \sinh(\gamma\tau_2)}{\sinh(\gamma\tau)} \left( \frac{1}{\Gamma_1} - \frac{1}{\Gamma_2} \right)^2, \quad (28)$$

which it is strictly positive (as expected). The component  $(1/\Gamma_1 - 1/\Gamma_2)$  can be regarded as the ‘‘thermodynamic force’’  $f_T$  associated with the difference of temperature of the reservoirs. Particularly, in the linear regime ( $\Gamma_2 \simeq \Gamma_1 = \Gamma$ ),  $\bar{\Pi}_T$  can be conveniently written down in terms of Onsager coefficient  $\bar{\Pi}_T = L_{T\Gamma} f_T$ , where  $L_{T\Gamma}$  is given by,

$$L_{T\Gamma} = k_B \frac{\Gamma^2}{\tau} \frac{\sinh(\gamma\tau_1) \sinh(\gamma\tau_2)}{\sinh(\gamma\tau)}. \quad (29)$$

Note that  $L_{T\Gamma}$  is strictly positive and it reduces to  $k_B \Gamma^2 \tanh[\frac{\gamma\tau}{2}]/2\tau$  for  $\tau_1 = \tau_2$  (symmetric case). Further, it is straightforward to verify that the dissipation term  $\bar{\Pi}_T$  is a monotonous decreasing function of  $\tau$  and it is always larger for the symmetric case ( $\tau_1 = \tau_2$ ). Both properties of  $\bar{\Pi}_T$  are illustrated in Fig. 1, where  $\bar{\Pi}_T$  is shown as a function of  $\tau$  for various values of the asymmetry parameter  $\kappa = \tau_1/\tau_2$  (notice that  $\bar{\Pi}_T$  is invariant over the switch of the interaction times  $\tau_1 \leftrightarrow \tau_2$  or, equivalently  $\kappa \leftrightarrow 1/\kappa$ ). There is one caveat which concerns the validity of the results of Fig. 1. Collisional models usually neglects the time for changing the contact between the system and thermal baths. However, if  $\tau$  is very small, such approximation can no longer be hold. We shall assume along this paper that  $\tau$  is large enough for the collisional approximation to be valid.

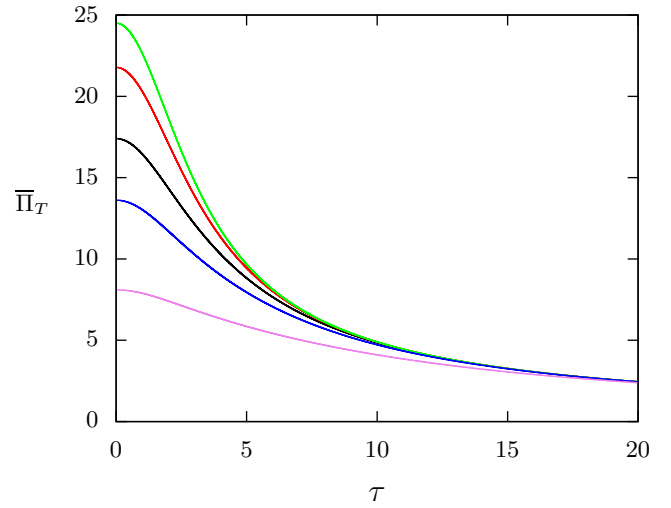


FIG. 1. Mean entropy production component  $\bar{\Pi}_T$  as a function of the period  $\tau$  for  $\gamma = 1$ ,  $\Gamma_1 = 1$  and  $\Gamma_2 = 100$  and distinct asymmetries. From top to bottom:  $\kappa = 1.0, 0.5, 0.3, 0.2$  and  $0.1$ .

The entropy production component coming from external forces also assumes a general (bilinear) form given by,

$$\bar{\Pi}_F = \tilde{L}_{11} X_1^2 + (\tilde{L}_{12} + \tilde{L}_{21}) X_1 X_2 + \tilde{L}_{22} X_2^2. \quad (30)$$

The coefficients  $\tilde{L}_{ij}$ 's are shown in the Appendix A, Eq. (A2). It should be noticed that Eq. (30) is exact for all force regimes (not only in the linear regime). For equal temperatures, they coincide with Onsager coefficients [Eq. (24)]. A detailed analysis for distinct linear regimes (low temperature difference and/or low forces) is undertaken in Appendix A. Furthermore, since  $\tau_2 = \tau - \tau_1$ , the coefficients above fulfill the reciprocal relations  $\tilde{L}_{11} \leftrightarrow \tilde{L}_{22}$  and  $\tilde{L}_{12} \leftrightarrow \tilde{L}_{21}$  by exchanging  $1 \leftrightarrow 2$  for the generic drivings  $g_i(t)$ 's, the interaction times  $\tau_i$ 's and the temperature of the reservoirs  $T_i$ 's.

### III. EFFICIENCY

The optimization of engines, which converts energy (usually heat or chemical work) into mechanical work, constitutes one of the main issues in thermodynamics, engineering, chemistry and others. Here we exploit the role of asymmetric contact times between the Brownian particle and the thermal reservoirs as a reliable strategy for optimizing the machine performance. More specifically, the amount of energy (heat and work) received by the particle is partially converted into output work (or, equivalently, the output power per cycle)  $\mathcal{P} = \bar{W}_2 \geq 0$  during the second half stage. A measure of efficiency is given by the ratio of the amount of output work to the total energy injected

$$\eta = -\frac{\mathcal{P}}{\bar{W}_1 + \bar{Q}_i}, \quad (31)$$

where  $\bar{Q}_i$  is the average heat extracted from the reservoir  $i$  ( $i = 1$  or  $2$  whether the reservoir 1 or 2 delivers heat to the

Brownian particle), whereas for the other way round (both reservoirs absorbing energy from the particle),  $\bar{Q}_i$  does not appear in Eq. (31), as shall be discussed in Sec. III A. Below, we are going to investigate the machine optimization with respect to the loading force  $X_2$  and asymmetry coefficient  $\kappa = \tau_1/\tau_2$  for two distinct scenarios: equal and different temperatures.

### A. Isothermal work-to-work converter

Many processes in nature, such as biological systems, operate at homogeneous (or approximately equal) temperatures, in which an amount of chemical work/energy is converted into mechanical work and vice-versa (see e.g. [41, 42]). This highlights the importance of searching for optimized protocols operating at equal temperatures. Here we exploit the present Brownian machine operating at equal temperatures, but subject to distinct external forces. From Eqs. (11) and (19), it follows that  $\bar{Q}_1 \geq 0$  and  $\bar{Q}_2 \geq 0$  and therefore no heat is delivered to the particle. Such engine reduces to a work-to-work converter: the particle receives input power  $\bar{W}_1 < 0$  which is partially converted into output power  $\mathcal{P} \geq 0$ . From Eq. (24), the output power and efficiency can be expressed in terms of the Onsager coefficients according to the following expressions:

$$\mathcal{P} = \bar{W}_2 = -k_B T \left[ L_{22}(\kappa) X_2^2 + L_{21}(\kappa) X_1 X_2 \right]. \quad (32)$$

and

$$\eta = -\frac{L_{21} X_1 X_2 + L_{22} X_2^2}{L_{11} X_1^2 + L_{12} X_1 X_2}, \quad (33)$$

Both of them can be expressed in terms of the ratio  $X_2/X_1$  between forces, the output power being a function of such ratio multiplied by  $X_1^2$ . As mentioned previously, there are three routes to be considered with respect to the engine optimization (holding  $X_1$  and  $\tau$  fixed): the time asymmetry optimization (conveniently carried out in terms of ratio  $\kappa = \tau_1/\tau_2$ ), the output force  $X_2$  optimization; and both optimizations together. We shall analyze all cases in the following subsections.

#### 1. Maximization with respect to the asymmetry

Since the Brownian particle must be in contact with the first reservoir long enough for the injected energy to be larger than the energy dissipated by the viscous force, for any set of  $X_1$  and  $X_2$  there is a minimum value  $\kappa_m$  for which  $\mathcal{P} \geq 0$ . On the other hand, depending on the kind of driving, it can extend up to  $\kappa \rightarrow \infty$ , for which  $L_{21}$  and  $L_{22}$  vanishes [see Eq. (24)].

The choice of optimal asymmetries are expected to be dependent of the quantity chosen to be maximized. Usually, there are two quantities of interest: maximum efficiency or maximum power output. Starting with the latter case, the optimal asymmetry  $\kappa_{MP}$  which maximizes  $\mathcal{P}$  is the solution of following equation

$$\frac{L'_{21}(\kappa_{MP})}{L'_{22}(\kappa_{MP})} = -\frac{X_2}{X_1}, \quad (34)$$

where  $L'_{ij}(\kappa) \equiv \partial L_{ij}(\kappa)/\partial \kappa$  and in this section  $L_{ij}$ 's (together their derivatives) have been expressed in terms of  $\kappa$  for specifying which quantity ( $\mathcal{P}$  or  $\eta$ ) has been maximized. In general, Eq. (34) may have more than one solution for each choice of the ratio  $X_2/X_1$  and one should be careful to identify the global maximum. However, in the following discussion (as in the examples presented in Section III A 3), we consider the cases which present a single maximum.

Similarly, from Eq. (33), we obtain the value of the asymmetry that maximizes the efficiency  $\kappa_{M\eta}$  from the transcendental equation

$$\Delta_{2212}(\kappa_{M\eta}) X_2^2 + \Delta_{2111}(\kappa_{M\eta}) X_1^2 + \left[ \Delta_{2211}(\kappa_{M\eta}) + \Delta_{2112}(\kappa_{M\eta}) \right] X_1 X_2 = 0, \quad (35)$$

where  $\Delta_{ijkl}(\kappa) = L'_{ij}(\kappa)L_{kl}(\kappa) - L'_{kl}(\kappa)L_{ij}(\kappa)$ . Although exact, for a given choice of the drivings  $g_i(t)$  and the strengths  $X_i$ , Eqs. (34) and (35), in general, have to be solved numerically for  $\kappa_{MP}$  and  $\kappa_{M\eta}$ , respectively. After these values are obtained, we can evaluate the power  $\mathcal{P}_{MP,\kappa}$  and efficiency  $\eta_{MP,\kappa}$  at maximum power as

$$\mathcal{P}_{MP,\kappa} = \frac{k_B T L'_{21}(\kappa_{MP})}{L_{22}^2(\kappa_{MP})} [L_{21}(\kappa_{MP}) L'_{22}(\kappa_{MP}) - L_{22}(\kappa_{MP}) L'_{21}(\kappa_{MP})] X_1^2, \quad (36)$$

and

$$\eta_{MP,\kappa} = \frac{L'_{21}(\kappa_{MP}) [L'_{22}(\kappa_{MP}) L_{21}(\kappa_{MP}) - L_{22}(\kappa_{MP}) L'_{21}(\kappa_{MP})]}{L'_{22}(\kappa_{MP}) [L_{11}(\kappa_{MP}) L'_{22}(\kappa_{MP}) - L_{12}(\kappa_{MP}) L'_{21}(\kappa_{MP})]}. \quad (37)$$

Analogously, we can write the power at maximum efficiency  $\mathcal{P}_{M\eta,\kappa}$  and maximum efficiency  $\eta_{M\eta,\kappa}$  as

$$\mathcal{P}_{M\eta,\kappa} = -k_B T \left[ L_{22}(\kappa_{M\eta}) X_2^2 + L_{21}(\kappa_{M\eta}) X_1 X_2 \right], \quad (38)$$

and

$$\eta_{M\eta,\kappa} = -\frac{L_{22}(\kappa_{M\eta}) X_2^2 + L_{21}(\kappa_{M\eta}) X_1 X_2}{L_{11}(\kappa_{M\eta}) X_1^2 + L_{12}(\kappa_{M\eta}) X_1 X_2}, \quad (39)$$

respectively. In Sec III A 3, we will exemplify our exact expressions for maximum efficiencies and powers for two kinds of drivings.

#### 2. Maximization with respect to the output force

For given asymmetry and drivings, the Onsager coefficients are constant. Hence, the maximization of the output power and the efficiency turn out to be similar to the approach from Refs. [16, 33]. Below, we recast the main results.

As previously, the engine regime ( $\mathcal{P} > 0$ ) also imposes boundaries to optimization with respect to the force strength. Here, the output force  $X_2$  must lie in the interval  $X_m \leq X_2 \leq 0$ , where  $X_m = -L_{21} X_1 / L_{22}$ . In general,  $X_m$  is different from the value of the output force that minimizes the entropy production  $X_{2mS}$  (for  $X_1$  and  $\kappa$  constants). However, they coincide  $X_m = X_{2mS}$  for symmetric Onsager coefficients  $L_{12} = L_{21}$ .

Similarly to the previous subsection, the optimization can be performed to ensure maximum power  $\mathcal{P}_{MP,X_2}$  (with efficiency  $\eta_{MP,X_2}$ ) or maximum efficiency  $\eta_{M\eta,X_2}$  (with power  $\mathcal{P}_{M\eta,X_2}$ ), by adjusting the output forces to optimal values  $X_{2MP}$  and  $X_{2M\eta}$ , respectively. These optimal output forces can be expressed in terms of the Onsager coefficients as

$$X_{2M\eta} = \frac{L_{11}}{L_{12}} \left( -1 + \sqrt{1 - \frac{L_{12}L_{21}}{L_{11}L_{22}}} \right) X_1, \quad (40)$$

and

$$X_{2MP} = -\frac{1}{2} \frac{L_{21}}{L_{22}} X_1, \quad (41)$$

respectively. Hence, the maximum efficiency  $\eta_{M\eta,X_2}$  and the efficiency at maximum power  $\eta_{MP,X_2}$  are given by,

$$\eta_{M\eta,X_2} = -\frac{L_{21}}{L_{12}} + \frac{2L_{11}L_{22}}{L_{12}^2} \left( 1 - \sqrt{1 - \frac{L_{12}L_{21}}{L_{11}L_{22}}} \right), \quad (42)$$

and

$$\eta_{MP,X_2} = \frac{L_{21}^2}{4L_{11}L_{22} - 2L_{12}L_{21}}, \quad (43)$$

while the power at maximum efficiency  $\mathcal{P}_{M\eta,X_2}$  and the maximum power  $\mathcal{P}_{MP,X_2}$  can be obtained by inserting  $X_{2M\eta}$  or  $X_{2MP}$  into the expression for  $\mathcal{P}$ . In fact, these quantities are not independent of each other, instead they are related as

$$\eta_{MP,X_2} = \frac{\mathcal{P}_{MP,X_2}}{2\mathcal{P}_{MP,X_2} - \mathcal{P}_{M\eta,X_2}} \eta_{M\eta,X_2}. \quad (44)$$

Furthermore, for symmetric Onsager coefficients  $L_{12} = L_{21}$ , there two additional simple relations given by,

$$\eta_{MP,X_2} = \frac{\eta_{M\eta,X_2}}{1 + \eta_{M\eta,X_2}^2} \quad \text{and} \quad \frac{\mathcal{P}_{M\eta,X_2}}{\mathcal{P}_{MP,X_2}} = 1 - \eta_{M\eta,X_2}^2. \quad (45)$$

As shown in Appendix B,  $L_{12} = L_{21}$  for constant drivings for any value of  $\kappa$ . Conversely, they are in general different ( $L_{12} \neq L_{21}$ ) for linear drivings (see Appendix C). For the symmetric time case ( $\kappa = 1$ ), however, the equality holds also for linear drivings [33].

### 3. Constant and linear drivings

In order to access the advantages of the asymmetry in the time spent by the Brownian particle in contact with each reservoir, we consider two different driving models. In the first model, the drivings are constant and the external forces can be written as

$$f_1(t) = X_1, \quad \text{for } 0 \leq t < \tau_1 \quad (46)$$

$$f_2(t) = X_2, \quad \text{for } \tau_1 \leq t < \tau. \quad (47)$$

In Appendix B, we present explicit expressions for the average velocities  $\langle v_i \rangle(t)$  and Onsager coefficients  $L_{ij}$  (which coincides with the coefficients  $\tilde{L}_{ij}$  for isothermal reservoirs). The

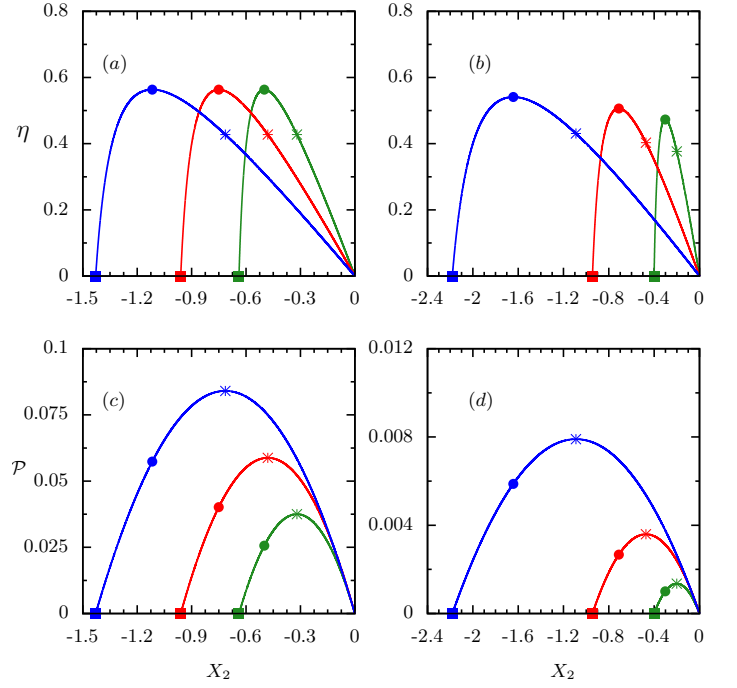


FIG. 2. Efficiency [panels (a) and (b)] and output power [panels (c) and (d)] (averaged over one period) for the isothermal work-to-work converter with  $X_1 = 1$ ,  $\tau = 1$ ,  $\gamma = 1$  and different asymmetries  $\kappa$  (from left to right,  $\kappa = 1.50$ ,  $1.00$  and  $0.67$ ). Panels (a) and (c) depict the results for constant drivings, whereas (b) and (d) for the linear drivings one. In all panels, squares, circles and stars denote  $X_{2ms}$ ,  $X_{2M\eta}$  and  $X_{2MP}$ , respectively.

second class of Brownian engines deals with drivings evolving linearly in time and given by the following expressions

$$f_1(t) = X_1\gamma t, \quad \text{for } 0 \leq t < \tau_1 \quad (48)$$

$$f_2(t) = X_2\gamma(t - \tau_1), \quad \text{for } \tau_1 \leq t < \tau. \quad (49)$$

The main expressions for such case are listed in Appendix C. Figs. 2 and 3 depict typical plots of the efficiency and power output for both force models as a function of the output force  $X_2$  and asymmetry  $\kappa$ , respectively.

As discussed above, the engine regime operates for  $X_{2m} < X_2 < 0$ . An immediate advantage of the time asymmetry concerns the minimum output forces  $X_{2m}$  which decreases with  $\kappa$ , implying that the engine regime interval increases with the asymmetry (see Fig. 2). Such trend is consistent with the absorption of energy (average work rate  $\overline{W}_1$ ) for longer and longer time as  $\kappa$  increases. Furthermore, the minimum entropy production (represented by the squares in the figure) coincides with the minimum loading force (vanishing power output and efficiency) for constant drivings, but not for the linear case (although  $X_{2ms}$  is close to  $X_m$ ).

The maximum efficiencies are almost constant for the constant force model [Fig. 2(a)] and slightly increase with  $\kappa$  [Fig. 2(b)] for the linear force model. However, for small  $|X_2|$ , the efficiency is larger for the smaller values of  $\kappa$ . The effect of the time asymmetry for the output power is more pronounced. For both force models, the maximum power output clearly in-

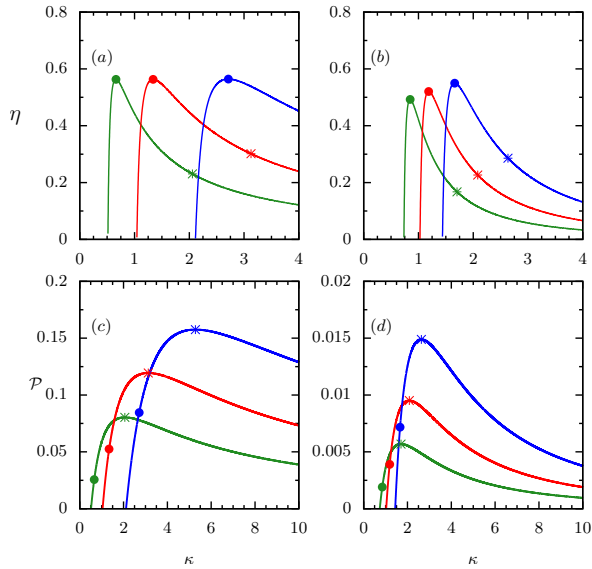


FIG. 3. Efficiency [panels (a) and (b)] and output power [panels (c) and (d)] (averaged over one period) for the isothermal work-to-work converter with  $X_1 = 1$ ,  $\tau = 1$ ,  $\gamma = 1$  and different values of  $X_2$  (from left to right,  $X_2 = -0.5, -1.0$  and  $-2.0$ ). Panels (a) and (c) depict the main results for the constant drivings model while (b) and (d) the linear drivings one. In all panels, circles and stars denote  $\kappa_{2M\eta}$  and  $\kappa_{2MP}$ , respectively. For such set of parameters, the associate  $\kappa_{2mS}$ 's are out of the engine regime.

creases with  $\kappa$ .

Fig. 4 depicts, for constant and linear drivings, a heat map for the power output and efficiency as a function of both the asymmetry and loading forces. For aesthetic reasons, they have been expressed in terms  $1/\kappa$  (instead of  $\kappa$ ) in the vertical axis. Noteworthy, the maximum efficiency curves, represented by the dashed (full) line for the maximization with respect to  $\kappa$  (loading force), are close to each other. Consequently, the choice of the parameter to maximize the efficiency is not important for both models presented here. Moreover, as previously discussed, the maximum efficiency is almost constant for the constant drivings model, but increases with  $\kappa$  for the linear drivings one. In contrast to the maximum efficiencies, maximum power curves (panels 4(a) and 4(c) for constant and linear drivings, respectively) present rather different behaviors depending on the optimization parameter. The  $\mathcal{P}_{MP,\kappa}$  curves (dashed lines) always lie above the  $\mathcal{P}_{MP,X_2}$  (full lines) ones and they approach each other as  $\kappa \rightarrow \infty$ . Finally, it is worth pointing out that while both drivings provide similar efficiencies, the constant driving case is clearly more advantageous than the linear one in terms of the output power.

#### 4. Simultaneous maximization of the asymmetry and the force

One may also raise the relevant issue of maximizing the power output and efficiency with respect to the asymmetry and output force strength simultaneously. Although this is not possible in some cases (as explained below), we will proceed

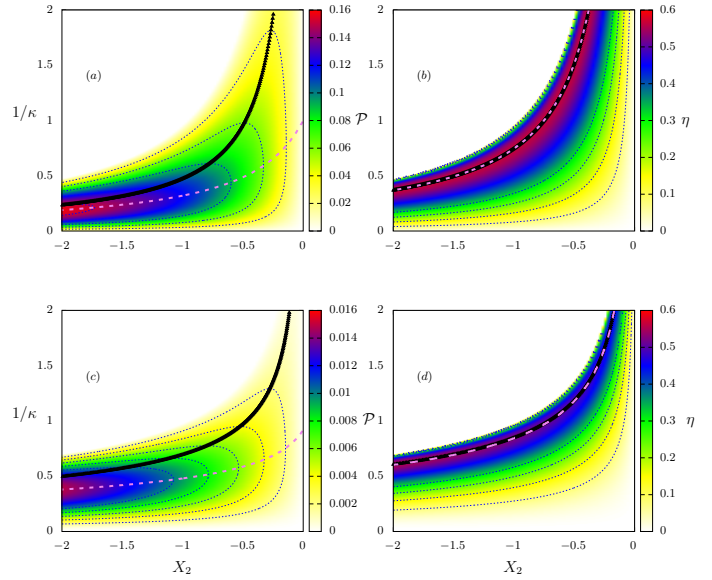


FIG. 4. For the isothermal work-to-work converter, the output power (left panels) and efficiency (right panels) for the constant [(a) and (b)] and linear [(c) and (d)] drivings models as a function of the inverse of the asymmetry parameter  $\kappa$  and loading forces  $X_2$ . Dotted lines represent constant value loci, dashed and full lines represent maximization with respect to  $\kappa$  and  $X_2$ , respectively. Parameters:  $\tau = 1$ ,  $\gamma = 1$ ,  $X_1 = 1$ .

presenting the framework assuming that such maximization is possible. As before, we shall restrict the analysis to drivings presenting a single physical solution for Eqs. (34) and (35). If this is not the case, each maximum of these equations should be analyzed individually to assert which is the global maximum in each case.

Under the assumption above, the maximum power output must satisfy simultaneously Eqs. (34) and (41), that is, we must find the optimal value of the asymmetry  $\kappa_{MP}^*$  which satisfy the following condition:

$$\frac{L'_{21}(\kappa_{MP}^*)}{L'_{22}(\kappa_{MP}^*)} = \frac{1}{2} \frac{L_{21}(\kappa_{MP}^*)}{L_{22}(\kappa_{MP}^*)}. \quad (50)$$

Once the optimal asymmetry  $\kappa_{MP}^*$  is obtained, the optimal force  $X_{2MP}^*$  is calculated from Eq. (41) and given by

$$X_{2MP}^* = -\frac{1}{2} \frac{L_{21}(\kappa_{MP}^*)}{L_{22}(\kappa_{MP}^*)} X_1. \quad (51)$$

Graphically, the condition above is precisely the crossing point between lines for which the power (or efficiency) is maximized with respect to  $X_2$  and  $\kappa$ . However, in some cases, (as illustrated by the constant and linear drivings presented above) these two lines do not cross at all. The physical reason is that the power output keeps growing as  $\kappa \rightarrow \infty$  (with an appropriate choice of a value of  $X_2$  for each  $\kappa$ ). In other words, for such models, it is advantageous to apply a very large output force (in modulus) for a short period. Conversely, if the force model involves a rapidly decaying input driving  $g_1(t)$  and growing output driving  $g_2(t)$ , an optimal output power may be found.

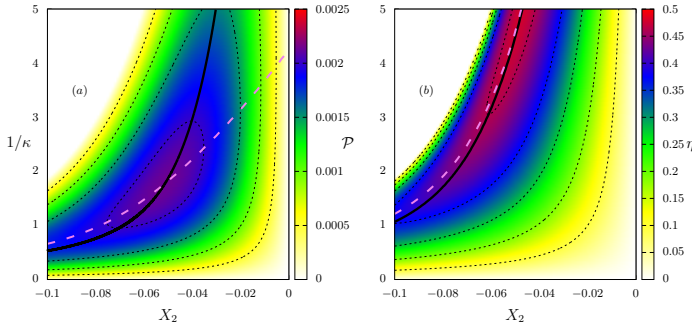


FIG. 5. For the exponential driving, depiction of output power (a) and efficiency (b) versus the inverse of the asymmetry coefficient  $\kappa$  and the output force  $X_2$  for  $\tau = 1$ ,  $\gamma = 1$  and  $X_1 = 1$ . Dotted lines represent constant value loci, dashed and solid lines represent maximization with respect to  $\kappa$  and  $X_2$ , respectively.

In such case, the power and efficiency at maximum power are readily evaluated as

$$\mathcal{P}^* = \frac{k_B T}{4} \frac{L_{21}^2(\kappa_{MP}^*)}{L_{22}(\kappa_{MP}^*)} X_1^2, \quad (52)$$

and

$$\eta^* = \frac{L_{21}^2(\kappa_{MP}^*)}{4L_{11}(\kappa_{MP}^*)L_{22}(\kappa_{MP}^*) - 2L_{21}(\kappa_{MP}^*)L_{12}(\kappa_{MP}^*)}. \quad (53)$$

Thereby, the optimal output power increases quadratically with the input force while the efficiency is completely determined by the driving force model. It is noteworthy that, despite the apparent temperature dependency of the power output in Eq. (52), the temperature cancels out when we use the expressions for the Onsager coefficients [see e.g. Eq. (24)]. Similar expressions can be obtained for the simultaneous maximization of efficiency [by equaling the ratio  $X_2/X_1$  from Eqs. (35) and (40)]. Since expressions are more involved, we abstain to present them here. In order to illustrate the previous ideas, we consider an exponential driving given by

$$f_1(t) = X_1 e^{-\gamma t}, \quad \text{for } 0 \leq t < \tau_1 \quad (54)$$

$$f_2(t) = X_2 e^{\gamma(t-\tau_1)}, \quad \text{for } \tau_1 \leq t < \tau. \quad (55)$$

Figs. 5 (a) and (b) depict, for above exponential drivings, the heat maps of the output power and efficiency as functions of  $\kappa$  and  $X_2$ , respectively. Contrasting to the previous models, the crossing between maximum power lines are evident for the exponential drivings model above and thereby the global optimization is possible. Although for the exponential model given by Eqs. (54) and (55) the crossing between maximum efficiency curves is absent, it does appear for other exponential drivings choices (e.g. for  $f_1(t) = X_1 e^{-\gamma t}$  and  $f_2(t) = X_2 e^{3\gamma(t-\tau_1)}$ ) and follow theoretical prescription above.

## B. Thermal engine

In this section, we derive general findings for thermal engines in which the particle is also exposed to distinct thermal

baths in each stage. Although the power output  $\mathcal{P}$  is the same as before (it does not depend on the temperatures), the efficiency may change because of the appearance of heat flow. Hence, in addition to the input energy received as work, the engine may also receive energy from the hot reservoir. Consequently, the maximization of power output with respect to the output force  $X_{2MP}$  or the asymmetry  $\kappa_{MP}$  is the same as before, but the corresponding efficiencies may differ (if  $\bar{Q}_1 < 0$  or  $\bar{Q}_2 < 0$ ) from such case, following Eq. (31) instead. Anyhow, the efficiency of the engine for reservoirs with different temperatures is always smaller or equal than for isothermal reservoirs.

From Eq. (11), the average heat dissipated by the Brownian particle per cycle while in contact with the  $i$ -reservoir  $\bar{Q}_i$  can be obtained as

$$\bar{Q}_1 = \frac{m\gamma}{\tau} \left[ \int_0^{\tau_1} \langle v_1 \rangle^2 dt - C(\tau_1)(\Gamma_1 - \Gamma_2) \right], \quad (56)$$

$$\bar{Q}_2 = \frac{m\gamma}{\tau} \left[ \int_{\tau_1}^{\tau} \langle v_2 \rangle^2 dt + C(\tau_1)(\Gamma_1 - \Gamma_2) \right], \quad (57)$$

where  $C(\tau_1) = \text{csch}(\gamma\tau) \sinh(\gamma\tau_1) \sinh(\gamma(\tau-\tau_1))/2\gamma^2$  is strictly positive. Therefore, since the first term on the right-hand side of Eqs. (56) and (57) are positive, heat always flow into the colder reservoir. As about the hot reservoir, the heat may flow from or into the reservoir. For simplicity, we shall restrict our analysis to the case  $\Gamma_1 > \Gamma_2$ , that is, the first reservoir being the hot one, but it is worth pointing out that all the discussion below holds valid for  $\Gamma_1 < \Gamma_2$  if we analyze Eq. (57) instead of Eq. (56).

For  $\Gamma_1 > \Gamma_2$ , Eq. (56) ensures that heat flows into the system if  $\int_0^{\tau_1} \langle v_1 \rangle^2 dt < C(\tau_1)(\Gamma_1 - \Gamma_2)$ . Physically, this condition is a balance between kinetic energy that flows into the system due to the forces and the dissipation. If  $X_1$  is strong enough (or if the difference of temperature of the reservoirs is small enough), energy flows into both reservoirs. Thereby, the engine effectively reduces to an isothermal work-to-work converter, so that the efficiency is still described by Eq. (33) and all results and findings from Section III A regarding the efficiency optimization hold. Otherwise, the inequality above is satisfied and energy flows from the first reservoir into the engine. For  $\Gamma_1 < \Gamma_2$ , the same energy balance occurs, but we need to assert the positiveness or negativeness of Eq. (57).

Furthermore, although exact, the achievement of general expressions for optimized efficiencies outside the isothermal work-to-work regime is more cumbersome than the ones obtained for such regime, making a general analysis unfeasible. Nevertheless, the discussion of a simple asymptotic limit is instructive. If the second term on the right-hand side of Eq. (56) [or Eq. (57)] is the dominant one,  $|\Gamma_1 - \Gamma_2| \gg 1$  and  $|\bar{Q}_1| \gg |\bar{W}_2|$  [or  $|\bar{Q}_2| \gg |\bar{W}_2|$ ]. Therefore, the efficiency becomes  $\eta \approx -\mathcal{P}/\bar{Q}_1$  [or  $\eta \approx -\mathcal{P}/\bar{Q}_2$ ], which maximization, with respect to  $X_2$ , yields  $X_{2M\eta} \approx X_{2MP}$  and follows Eq. (41). Hence, the corresponding  $\eta_{M\eta}$  approaches to the following expression

$$\eta_{M\eta, X_2} \approx \frac{T_2}{8\gamma^2 T_i C(\tau_1)} \frac{L_{21}^2}{L_{22}} \tau X_1^2 \ll 1, \quad (58)$$



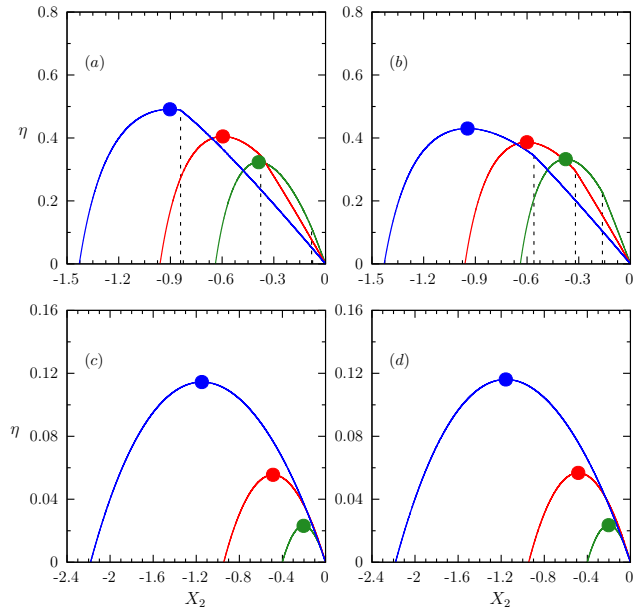


FIG. 6. Efficiency as a function of the force strength  $X_2$  for the constant [(a) and (b)] and linear [(c) and (d)] drivings, respectively. Parameters:  $\tau = 1$ ,  $\gamma = 1$  and  $X_1 = 1$  and distinct temperatures [ $\Gamma_1 = 2.0$  and  $\Gamma_2 = 1.5$  in panels (a) and (c) and  $\Gamma_1 = 1.5$  and  $\Gamma_2 = 2.0$  in panels (b) and (d)]. Circles denote maximum efficiencies and their  $X_{2MP}$ 's are the same as in Fig. 2. From left to right,  $\kappa = 1.50$ ,  $1.00$  and  $0.67$ ). Dashed vertical lines stands for the value of  $X_2$  for which  $\bar{Q}_i$  changes sign ( $i$  being the index of the hot reservoir).

where  $T_i$  is the temperature of the hot reservoir. When the hot bath is the first reservoir, the fact that the efficiency is small is direct since the factor  $T_2/T_1 \ll 1$ . However, when the second reservoir is the hotter one, the temperature ratio becomes 1 and the smallness of the efficiency comes from the Onsager coefficients:  $L_{21}^2/L_{22} \propto 1/T_2$ . It is also worth mentioning that the apparent dependence on the period cancels out because the Onsager coefficients are proportional to  $1/\tau$  [see Eq. (24)]. Therefore, for high temperature differences, the engine efficiency is very small for any value of the asymmetry.

In order to illustrate our findings for reservoirs with different temperatures, we consider the constant and linear drivings models presented above. Fig. 6 exemplifies, for distinct temperature reservoirs, the efficiency for the same values of  $\kappa$  used in Fig. 2 for constant [panels (a) and (b)] and linear drivings [panels (c) and (d)], respectively. In panels (a) and (c) the temperature of the first reservoir is larger than that of the second reservoir, while panels (b) and (d) depict the other way around.

In accordance with general findings from Sec. III B, for constant drivings there are two regimes (the vertical lines in the figure denotes the value of  $X_2$  which separates them) for which the heat exchanged between the Brownian particle and the hot reservoir changes sign. Conversely, they are not present for the linear drivings model – panels (c) and (d)

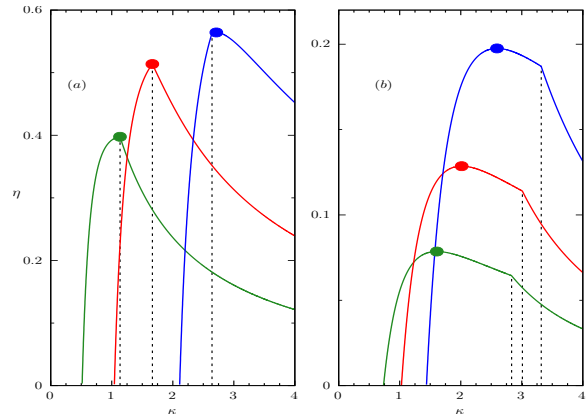


FIG. 7. Efficiency versus the time asymmetry  $\kappa$  for the (a) constant and (b) linear drivings, respectively, for  $\tau = 1$ ,  $\gamma = 1$  and  $X_1 = 1$  and different temperatures [ $\Gamma_1 = 2.0$  and  $\Gamma_2 = 1.5$ ]. Circles denote maximum efficiencies and their  $X_{2MP}$ 's are the same as in Fig. 3. From left to right,  $X_2 = -0.5$ ,  $-1.0$  and  $-2.0$ . Dashed vertical lines stands for the value of  $\kappa$  for which  $\bar{Q}_1$  changes sign. For such set of parameters  $k_{2ms}$  are out of the engine regime.

– because the heat exchange with the hot reservoir does not change sign for the parameters used in the figures. Since  $\langle v_i \rangle^2$  increases with  $X_2^2$ , the term coming from the difference of temperatures in Eq.(56) dominates over it when  $|X_2|$  is small and hence the machine is less efficient than the isothermal work-to-work converter. Conversely, for large  $|X_2|$  the engine may become as efficient as the isothermal work-to-work converter if the exchanged heat with the hot reservoir change sign – left of the line in panels (a) and (b). Anyhow, by comparing the performance of isothermal with the different temperature case, we see that the decay of efficiency for linear drivings is more pronounced than for constant drivings.

As for isothermal reservoirs, the machine performance always improves as  $\kappa$  increases, encompassing not only an extension of its operation regime  $X_{2m}$  but it also presents a more pronounced increase of efficiencies, again, more substantial for linear drivings. Moreover, the asymmetry may be used to mitigate the drop in the efficiency produced by the different temperatures of the thermal reservoirs.

In Fig. 7, we show the efficiency as a function of the asymmetry for various values of  $X_2$ . Similarly to the previous figure, the vertical lines denote the values of  $\kappa$  for which the heat from the hot reservoir change sign and delimits the isothermal work-to-work converter regime. The discussion whether the isothermal work-to-work converter regime lies to the left or right of the vertical lines is not so obvious because both  $C(\tau_1)$  and  $\langle v_1 \rangle$  depend on the asymmetry. However, the work-to-work regime lies to the right of the lines, since the function  $C(\tau_1)$  reaches its maximum for  $\kappa = 1$  ( $\tau_1 = \tau/2$ ) and the first term on the right-hand side of Eq. (56) is expected to increase giving that its limit of integration increases with  $\kappa$ .

Fig. 8 presents heat maps of the efficiency for different temperature reservoirs as a function of the output force and asymmetry. By drawing a comparison with the isothermal work-

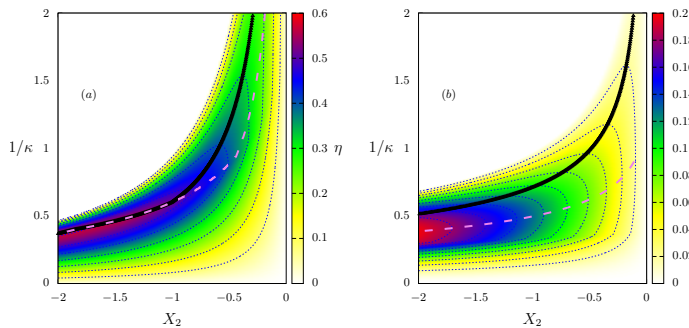


FIG. 8. Depiction of efficiency as a function of the inverse of the asymmetry coefficient  $\kappa$  and the output force  $X_2$ , for constant (a) and linear (b) drivings, respectively. Solid and dashed lines denote the maximization with respect to  $X_2$  and  $\kappa$ , respectively. Parameters:  $\Gamma_1 = 2.0$  and  $\Gamma_2 = 1.5$ ,  $\tau = 1$ ,  $\gamma = 1$  and  $X_1 = 1$ .

to-work converter (Fig. 4), it reveals that the difference of temperature makes the choice of the optimization parameter (force strength or time asymmetry) more relevant. While both optimized lines lie almost on top of each other for the isothermal case, Fig. 8 shows that they are clearly distinct, particularly for the linear drivings. Another point to be addressed concerns that high efficiencies are restricted to larger  $|X_2|$ 's for constant drivings when temperatures are different. This contrasts to its extension to smaller values for isothermal reservoirs [the hot (red) region in Fig. 4(b) is more spread than in Fig. 8(a)]. Conversely, for linear drivings, the decrease of the efficiency extends for all values of  $\kappa$  and  $X_2$  when compared with the isothermal work-to-work converter [note that efficiency in Fig. 4(d) is 3 times larger than Fig. 8(b)]. However, larger efficiencies in such case is obtained solely for larger values of  $|X_2|$  under a certain range of  $\kappa$ .

Lastly, we draw a comparison between the efficiency given by Eq. (31) with Eq. (45) from Ref. [33], which is based on the ratio between the entropy production fluxes. Although both expressions behave similarly and approach each other as  $\Delta\Gamma \rightarrow 0$  (or  $\Delta\Gamma \ll 1$ ), it is worth mentioning that the latter overestimates the efficiency as  $\Delta\Gamma$  increases.

#### IV. CONCLUSIONS

We introduced an alternative strategy for optimizing the performance of Brownian engines, based on the idea of asymmetric interaction time between the system (Brownian particle) and the thermal baths. Exact expressions for thermodynamic quantities and their maximized values were obtained, irrespective the kind of driving and asymmetry. The time asymmetry can always be tuned to obtain a gain larger than in the symmetric case. In addition to the improvement of the power output and efficiency, the time asymmetry also enlarges the range of forces for which the system operates as an engine. Another advantage of asymmetric times is that they can be conveniently chosen for compensating part of the limitations due the machine design, such as its operation period and

the driving considered.

Results for constant and linear drivings confirm that the appropriate tuning of the asymmetry produce gains for the efficiency substantially larger than those achieved for the symmetric case. Contrariwise to usual machines, for which the heat flow due to the gradient of temperature is fundamental for the power extraction and enhancing the efficiency, in the present case the efficiency is higher for isothermal reservoirs. The reason for such behavior concerns that the energy exchange between the Brownian particle and the different thermal reservoirs occurs in different stages. Since the heat transfer and the output force are uncoupled, the heat flux can not be converted into useful work. For instance, one would require drivings dependent of the velocity in order to be able to extract work from heat in the present model. Although the robustness of our findings has been verified for a few examples of drivings, our approach can be straightforwardly extended for other thermal machines, where in principle similar findings are expected. This is reinforced for recent results unveiling the importance of asymmetric times for optimizing the efficiency at maximum power of a quantum-dot thermal machine, which gain provides efficiencies larger than Curzon-Ahlborn [43].

We finish this paper highlighting a couple of perspectives. While in the present work we analyzed the maximization of the output power and efficiency with respect to the time asymmetry and the output force strength, keeping the other parameters of the machine fixed, it might be worth to study the maximization under different physical conditions, such as holding the dissipation or efficiency fixed. Finally, it might also be interesting to extend the role of asymmetric times for other kinds of drivings (e.g. velocity dependent drivings providing extraction of useful work from heat) as well as for massive Brownian particles (underdamped case) in order to compare their performances.

#### V. ACKNOWLEDGMENT

C. E. F acknowledges the financial support from FAPESP under grant 2018/02405-1. AR thanks Pronex/Fapesq-PB/CNPq Grant No. 151/2018 and CNPq Grant No. 308344/2018-9.

#### Appendix A: Onsager coefficients and linear regimes

In this appendix, we address the relation between coefficients  $\tilde{L}_{ij}$  and Onsager coefficients  $L_{ij}$ . Our starting point is the steady state entropy production averaged over one period which is given by,

$$\bar{\Pi} = \frac{2\gamma k_B}{m} \left( \frac{\bar{Q}_1}{\Gamma_1} + \frac{\bar{Q}_2}{\Gamma_2} \right) = \bar{\Pi}_F + \bar{\Pi}_T. \quad (\text{A1})$$

The coefficients  $\tilde{L}_{ij}$  are straightforwardly obtained from  $\bar{\Pi}_F$  performing the integration in Eq. (27), which  $\langle v_i \rangle(t)$ 's are given by Eq. (18), as:

$$\begin{aligned}
\tilde{L}_{11} &= \frac{\gamma}{\tau} \left[ \frac{(e^{2\gamma(\tau-\tau_1)} - 1) \hat{G}_1(\tau_1)^2}{\Gamma_2 (e^{\gamma\tau} - 1)^2} + \frac{\gamma}{\Gamma_1} \int_0^{\tau_1} \frac{2e^{-2\gamma t} [(e^{\gamma t} - 1) \hat{G}_1(t) + \hat{G}_1(\tau_1)]^2}{(e^{\gamma t} - 1)^2} dt \right] \\
\tilde{L}_{22} &= \frac{\gamma}{\tau} \left[ \frac{(1 - e^{-2\gamma\tau_1}) \hat{G}_2(\tau)^2}{\Gamma_1 (e^{\gamma\tau} - 1)^2} + \frac{\gamma}{\Gamma_2} \int_{\tau_1}^{\tau} \frac{2e^{-2\gamma t} [(e^{\gamma t} - 1) \hat{G}_2(t) + \hat{G}_2(\tau)]^2}{(e^{\gamma t} - 1)^2} dt \right], \\
\tilde{L}_{12} + \tilde{L}_{21} &= \frac{2\gamma e^{-\gamma\tau_1} \hat{G}_1(\tau_1) \hat{G}_2(\tau)}{\tau (e^{\gamma\tau} - 1)^2} \left[ \frac{\sinh(\gamma\tau_1)}{\Gamma_1} + \frac{\sinh(\gamma(\tau - \tau_1))}{\Gamma_2} \right] \\
&\quad + \frac{2\gamma^2}{\Gamma_1 \Gamma_2 \tau (e^{\gamma\tau} - 1)} \left[ \Gamma_2 \hat{G}_2(\tau) \int_0^{\tau_1} \hat{G}_1(t) e^{-2\gamma t} dt + \Gamma_1 \hat{G}_1(\tau_1) \int_{\tau_1}^{\tau} \hat{G}_2(t) e^{\gamma(\tau-2t)} dt \right],
\end{aligned} \tag{A2}$$

where  $\hat{G}_i(t) = \int_{\tau_{i-1}}^t g_i(t') dt'$ . For equal temperatures  $\Gamma_1 = \Gamma_2 = \Gamma$ ,  $\bar{\Pi}$  reduces to the following expression:

$$\begin{aligned}
\bar{\Pi} &= \bar{\Pi}_F = -\frac{2\gamma k_B}{m\Gamma} (\bar{W}_1 + \bar{W}_2) \\
&= L_{11} X_1^2 + (L_{12} + L_{21}) X_1 X_2 + L_{22} X_2^2.
\end{aligned} \tag{A3}$$

Hence, for isothermal reservoirs the entropy production can be written in terms of the Onsager coefficients even in the non-linear (force) regime and thereby  $\tilde{L}_{ij} = L_{ij}$ . Conversely, for the thermal linear regime, it is convenient to express  $\Gamma_1$  and  $\Gamma_2$  in terms of the difference of temperatures  $\Gamma_1 = \Gamma - \Delta\Gamma$  and  $\Gamma_2 = \Gamma + \Delta\Gamma$ . In such case, Eq. (A1) becomes

$$\bar{\Pi} \approx \frac{2\gamma k_B}{m\Gamma} \left[ -(\bar{W}_1 + \bar{W}_2) + (\bar{Q}_1 - \bar{Q}_2) \frac{\Delta\Gamma}{\Gamma} \right]. \tag{A4}$$

Let us assume that  $\tilde{L}_{ij}$  can be expanded in power series of the temperature difference,  $\tilde{L}_{ij} = L_{ij}^{(0)} + L_{ij}^{(c)} \Delta\Gamma$ , where  $L_{ij}^{(0)}$  is the coefficient for  $\Gamma_1 = \Gamma_2 = \Gamma$  and  $L_{ij}^{(c)}$  is the first order correction. In terms of such coefficients, the average entropy production  $\bar{\Pi}$  is given by

$$\begin{aligned}
\bar{\Pi} &= \bar{\Pi}_F + \bar{\Pi}_T \\
&= \left[ L_{11}^{(0)} X_1^2 + (L_{12}^{(0)} + L_{21}^{(0)}) X_1 X_2 + L_{22}^{(0)} X_2^2 \right] + \\
&\quad + \left[ L_{11}^{(c)} X_1^2 + (L_{12}^{(c)} + L_{21}^{(c)}) X_1 X_2 + L_{22}^{(c)} X_2^2 \right] \Delta\Gamma \\
&\quad + \frac{4L_{T\Gamma}}{\Gamma^2} (\Delta\Gamma)^2.
\end{aligned} \tag{A5}$$

By comparing Eqs. (A4) and (A5), it follows that

$$L_{11}^{(0)} X_1^2 + (L_{12}^{(0)} + L_{21}^{(0)}) X_1 X_2 + L_{22}^{(0)} X_2^2 = -\frac{2\gamma k_B}{m\Gamma} (\bar{W}_1 + \bar{W}_2), \tag{A6}$$

and hence Onsager coefficients  $L_{ij}$ 's correspond to 0-th order coefficients  $L_{ij}^{(0)}$ 's evaluated from  $\bar{\Pi}_F$ . Once again, they do not depend on  $\Delta\Gamma$ , since  $\bar{W}_i$  does not depend on the temperature at all.

In the true linear regime (both temperature gradient and force strength are small), the correction of  $\bar{\Pi}_F$  is of third order ( $X_i X_j \Delta\Gamma$ ), thus it can be neglected. Hence, the entropy

production components  $\bar{\Pi}_F$  and  $\bar{\Pi}_T$  are approximately

$$\bar{\Pi}_F \approx -\frac{2\gamma k_B}{m\Gamma} (\bar{W}_1 + \bar{W}_2), \tag{A7}$$

and

$$\bar{\Pi}_T \approx \frac{4L_{T\Gamma}}{\Gamma^2} (\Delta\Gamma)^2, \tag{A8}$$

respectively. In addition, the coefficients  $\tilde{L}_{ij}$  and  $L_{ij}$  are approximately equal  $\tilde{L}_{ij} \approx L_{ij}$ .

## Appendix B: Constant drivings

For the machine operating at constant drivings, defined by the forces from Eqs. (46) and (47), the velocities  $\langle v_i \rangle(t)$ 's are given by

$$\langle v_1 \rangle(t) = \frac{X_1}{\gamma} + \frac{e^{-\gamma(t-\tau_1)} - e^{-\gamma(t-\tau)}}{e^{\gamma\tau} - 1} \frac{X_1 - X_2}{\gamma}, \tag{B1}$$

$$\langle v_2 \rangle(t) = \frac{X_2}{\gamma} + \frac{e^{-\gamma(t-\tau-\tau_1)} - e^{-\gamma(t-\tau)}}{e^{\gamma\tau} - 1} \frac{X_1 - X_2}{\gamma}, \tag{B2}$$

for  $i = 1$  and  $2$ , respectively. The associated Onsager coefficients are straightforwardly obtained from Eq. (24) and are given by

$$\begin{aligned}
L_{11} &= \frac{2\tau_1}{\Gamma_1\tau} - L_{12}, \\
L_{22} &= \frac{2\tau_2}{\Gamma_2\tau} - L_{21}, \\
L_{12} &= \frac{4 \operatorname{csch}\left(\frac{\gamma\tau}{2}\right) \sinh\left(\frac{\gamma\tau_1}{2}\right) \sinh\left(\frac{1}{2}\gamma\tau_2\right)}{\gamma\Gamma_1\tau}, \\
L_{21} &= \frac{4 \operatorname{csch}\left(\frac{\gamma\tau}{2}\right) \sinh\left(\frac{\gamma\tau_1}{2}\right) \sinh\left(\frac{1}{2}\gamma\tau_2\right)}{\gamma\Gamma_2\tau}.
\end{aligned} \tag{B3}$$

Furthermore, for isothermal reservoirs,  $L_{12}$  and  $L_{21}$  are equal for any value of asymmetry parameter  $\kappa = \tau_1/\tau_2$ .

## Appendix C: Linear drivings

Similarly to the constant drivings model, the average velocities for the linear driving model [defined by Eqs. (48) and (49)] is obtained from Eq. (18) and are given by

$$\langle v_1 \rangle(t) = \frac{1}{\gamma} \left\{ X_1(\gamma t - 1) + \frac{e^{-\gamma t}}{e^{\gamma t} - 1} \left\{ X_1 \left[ e^{\gamma t} + e^{\frac{\gamma \kappa \tau}{1 + \kappa}} \left( \frac{\gamma \kappa \tau}{1 + \kappa} - 1 \right) \right] - X_2 \left[ e^{\frac{\gamma \kappa \tau}{1 + \kappa}} + e^{\gamma t} \left( \frac{\gamma \tau}{1 + \kappa} - 1 \right) \right] \right\} \right\}, \quad (C1)$$

and

$$\langle v_2 \rangle(t) = \frac{1}{\gamma} \left\{ X_2 \left[ 1 - \gamma \left( t - \frac{\kappa \tau}{1 + \kappa} \right) \right] + \frac{e^{-\gamma \left( t - \frac{\kappa \tau}{1 + \kappa} \right)}}{e^{\gamma t} - 1} \left\{ X_1 \left[ e^{\frac{\gamma \tau}{1 + \kappa}} + e^{\gamma t} \left( \frac{\gamma \kappa \tau}{1 + \kappa} - 1 \right) \right] - X_2 \left[ e^{\frac{\gamma \tau}{1 + \kappa}} \left( \frac{\gamma \tau}{1 + \kappa} - 1 \right) + e^{\gamma t} \right] \right\} \right\}. \quad (C2)$$

Likewise, Onsager coefficients  $L_{ij}$ 's are also straightforwardly calculated from Eq. (24) and read

$$\begin{aligned} L_{11} &= \frac{2\gamma^3 \tau_1^3 + \left[ 6 - 3\gamma^2 \tau_1^2 \right] \coth\left(\frac{\gamma \tau}{2}\right) + 6 \operatorname{csch}\left(\frac{\gamma \tau}{2}\right) \left[ \gamma \tau_1 \sinh\left(\frac{\gamma(\tau_1 - \tau_2)}{2}\right) - \cosh\left(\frac{\gamma(\tau_1 - \tau_2)}{2}\right) \right]}{3\gamma \Gamma \tau}, \\ L_{22} &= \frac{2\gamma^3 \tau_2^3 + \left[ 6 - 3\gamma^2 \tau_2^2 - 6 \cosh(\gamma \tau_1) \right] \coth\left(\frac{\gamma \tau}{2}\right) + 6\gamma \tau_2 \operatorname{csch}\left(\frac{\gamma \tau}{2}\right) \sinh\left(\frac{\gamma(\tau_2 - \tau_1)}{2}\right) + 6 \sinh(\gamma \tau_1)}{3\gamma \Gamma \tau}, \\ L_{12} &= \frac{2}{\gamma \tau \Gamma_1 (1 - e^{\gamma \tau})} \left[ 1 + \gamma \tau_1 - e^{\gamma \tau_1} \right] \left[ 1 - e^{\gamma \tau_2} (1 - \gamma \tau_2) \right], \\ L_{21} &= \frac{2}{\gamma \tau \Gamma_2 (1 - e^{\gamma \tau})} \left[ 1 + \gamma \tau_2 - e^{\gamma \tau_2} \right] \left[ 1 - e^{\gamma \tau_1} (1 - \gamma \tau_1) \right]. \end{aligned} \quad (C3)$$

Notably, contrasting to the constant drivings case, coefficients  $L_{12}$  and  $L_{21}$  are different from each other when  $\Gamma_1 = \Gamma_2$ . Only for symmetric switching times ( $\tau_1 = \tau_2$ ), it turns out that  $L_{12} = L_{21}$ .

- 
- [1] H. B. Callen, "Thermodynamics and an introduction to thermostatics," (1998).
- [2] I. Prigogine, *Introduction to thermodynamics of irreversible processes* (Interscience New York, 1965).
- [3] S. De Groot and P. Mazur, "North-holland," (1962).
- [4] U. Seifert, *Reports on progress in physics* **75**, 126001 (2012).
- [5] C. Van den Broeck, *Physical Review Letters* **95**, 190602 (2005).
- [6] G. Verley, M. Esposito, T. Willaert, and C. Van den Broeck, *Nature Communications* **5**, 4721 (2014).
- [7] T. Schmiedl and U. Seifert, *Europhysics Letters* **81**, 20003 (2007).
- [8] M. Esposito, K. Lindenberg, and C. Van den Broeck, *Physical Review Letters* **102**, 130602 (2009).
- [9] B. Cleuren, B. Rutten, and C. Van den Broeck, *The European Physical Journal Special Topics* **224**, 879 (2015).
- [10] M. Esposito, R. Kawai, K. Lindenberg, and C. Van den Broeck, *Physical Review E* **81**, 041106 (2010).
- [11] U. Seifert, *Physical Review Letters* **106**, 020601 (2011).
- [12] Y. Izumida and K. Okuda, *Europhysics Letters* **97**, 10004 (2012).
- [13] N. Golubeva and A. Imparato, *Physical Review Letters* **109**, 190602 (2012).
- [14] V. Holubec, *Journal of Statistical Mechanics: Theory and Experiment* **2014**, P05022 (2014).
- [15] M. Bauer, K. Brandner, and U. Seifert, *Physical Review E* **93**, 042112 (2016).
- [16] K. Proesmans, B. Cleuren, and C. Van den Broeck, *Physical review letters* **116**, 220601 (2016).
- [17] Z. Tu, *Journal of Physics A: Mathematical and Theoretical* **41**, 312003 (2008).
- [18] S. Ciliberto, *Physical Review X* **7**, 021051 (2017).
- [19] M. V. S. Bonança, *Journal of Statistical Mechanics: Theory and Experiment* **2019**, 123203 (2019).
- [20] B. Rutten, M. Esposito, and B. Cleuren, *Physical Review B* **80**, 235122 (2009).
- [21] K. Proesmans and C. Van den Broeck, *Chaos: An Interdisciplinary Journal of Nonlinear Science* **27**, 104601 (2017).
- [22] I. A. Martínez, É. Roldán, L. Dinis, D. Petrov, J. M. Parrondo, and R. A. Rica, *Nature Physics* **12**, 67 (2016).
- [23] K. Proesmans, Y. Dreher, M. c. v. Gavrilov, J. Bechhoefer, and C. Van den Broeck, *Phys. Rev. X* **6**, 041010 (2016).
- [24] S. Krishnamurthy, S. Ghosh, D. Chatterji, R. Ganapathy, and A. Sood, *Nature Physics* **12**, 1134 (2016).
- [25] V. Blickle and C. Bechinger, *Nature Physics* **8**, 143 (2012).
- [26] P. A. Quinto-Su, *Nature communications* **5**, 1 (2014).
- [27] A. Kumar and J. Bechhoefer, *Applied Physics Letters* **113**, 183702 (2018).
- [28] M. Esposito, R. Kawai, K. Lindenberg, and C. Van den Broeck, *Phys. Rev. Lett.* **105**, 150603 (2010).
- [29] T. Schmiedl and U. Seifert, *Phys. Rev. Lett.* **98**, 108301 (2007).
- [30] N. Pancotti, M. Scandi, M. T. Mitchison, and M. Perarnau-Llobet, *Phys. Rev. X* **10**, 031015 (2020).
- [31] N. Piccione, G. De Chiara, and B. Bellomo, *Phys. Rev. A* **103**, 032211 (2021).
- [32] P. Abiuso and M. Perarnau-Llobet, *Phys. Rev. Lett.* **124**, 110606 (2020).
- [33] A. L. L. Stable, C. E. F. Noa, W. G. C. Oropesa, and C. E. Fiore, *Phys. Rev. Research* **2**, 043016 (2020).
- [34] C. H. Bennett, *International Journal of Theoretical Physics* **21**, 905 (1982).
- [35] K. Maruyama, F. Nori, and V. Vedral, *Reviews of Modern Physics* **81**, 1 (2009).
- [36] T. Sagawa, *Journal of Statistical Mechanics: Theory and Experiment* **2014**, P03025 (2014).
- [37] J. M. Parrondo, J. M. Horowitz, and T. Sagawa, *Nature physics* **11**, 131 (2015).
- [38] T. Tomé and M. J. De Oliveira, *Stochastic dynamics and irreversibility* (Springer, 2015).

- [39] T. Tomé and M. J. de Oliveira, [Physical Review E](#) **82**, 021120 (2010).
- [40] T. Tomé and M. J. de Oliveira, [Physical review E](#) **91**, 042140 (2015).
- [41] S. Liepelt and R. Lipowsky, [Phys. Rev. E](#) **79**, 011917 (2009).
- [42] B. Altaner, A. Wachtel, and J. Vollmer, [Phys. Rev. E](#) **92**, 042133 (2015).
- [43] P. E. Harunari, F. S. Filho, C. E. Fiore, and A. Rosas, [Phys. Rev. Research](#) **3**, 023194 (2021).